Masaki Serizawa
Department of Mechanical Engineering,
Tokyo Denki University,
5 Senjyu Asahi-cho,
Adachi-ku, Tokyo 120-8551, Japan
e-mail: 12ky044@ms.dendai.ac.jp

Motohiro Suzuki
Department of Mechanical Engineering,
Tokyo Denki University,
5 Senjyu Asahi-cho,
Adachi-ku, Tokyo 120-8551, Japan
e-mail: kettle-on-the-stove@ezweb.ne.jp

Takashi Matsumura[1]
Mem. ASME
Department of Mechanical Engineering,
Tokyo Denki University,
5 Senjyu Asahi-cho,
Adachi-ku, Tokyo 120-8551, Japan
e-mail: tmatsumu@cck.dendai.ac.jp

Microthreading in Whirling

Whirling is applied to machining of microscrews on thin wires. A micro whirling machine has been developed for this. In order to suppress the vibration of the workpiece, the wire is inserted in polyurethane tubes clamped on a metal bar. Frequency analyses have been conducted by loading impulse forces at the center of the wire. The dynamic response is improved with reducing the vibration in the clamping force by the developed clamping system. Thirty micrometers microgrooves have been machined on 0.3 mm diameter stainless steel wires with fine surface finish, with the developed machine tool.
[DOI: 10.1115/1.4030704]

Introduction

Microscrews are used for mechanical joints and motion controls in microdevices. Stainless steel and titanium alloy, which are difficult-to-cut materials, are used in medical and dental devices because of their biocompatibility. Although, up to now, most micro-elements have been manufactured by chemical etching and energy beam processes, some manufacturing cost and production rate issues remain. More effective and flexible processes are required for the mass production of microparts. Micromechanical processing, one of the alternative processes, has remarkably progressed with the development of microtools and motion controls. Many studies of microscale cutting, forming, and injection molding have recently been applied to manufacturing of microparts [1,2].

Thread whirling, which is a material removal process with tool and workpiece rotations, has been applied to screw manufacturing in many mechanical industries, since it was developed by the Burgsmuller company in Germany. Worm and ball screws for motion controls and bone screws for the implant parts [3], which are made of hard materials, have been machined by whirling. Having many advantages in terms of tool wear and chip control, whirling has been widely applied in the bearing and the medical industries. Mohan and Shunmugam presented a mathematical model to control the cutting processes and determined the tool profiles in whirling [4]. Lee et al. presented a model of the uncut chip shape to estimate the cutting force from the maximum chip thickness and the tool-work contact length. They divided the uncut chip shape into the material removed by the front cutting edge and that by the side cutting edge; and estimated the cutting force by finite element (FE) analysis [5]. Song and Zuo proposed a novel model based on the equivalent cutting volume and simulated the chip formation in a FE commercial tool, AdvantEdge [6]. Son et al. measured the cutting force components with a noncontact rotating tool dynamometer and compared the measured force with the simulations using the FE analysis tools, DEFORM and ADAMS [7]. Guo et al. also analyzed the cutting tools' processing angle in whirling [8]. Although whirling is effective in threading, the screws are generally machined on large diameter shafts.

This study applies whirling to cutting threads on thin wires for micromechanical devices. The paper first presents an overview of whirling process along with its machining advantages. Based on the whirling mechanism, a micro whirling machine tool has been developed for machining microscrews on thin wires. Because the stiffness and the damping of the thin wire are low, a clamping device has also been developed to support the wire. Vibration tests have been conducted to verify improvement of the dynamic response of the workpiece with the clamping device.

Microscrews have been machined on 0.3 mm diameter titanium alloy and stainless steel wires with fine surfaces, using the developed machine tool. A mechanistic model is described to obtain

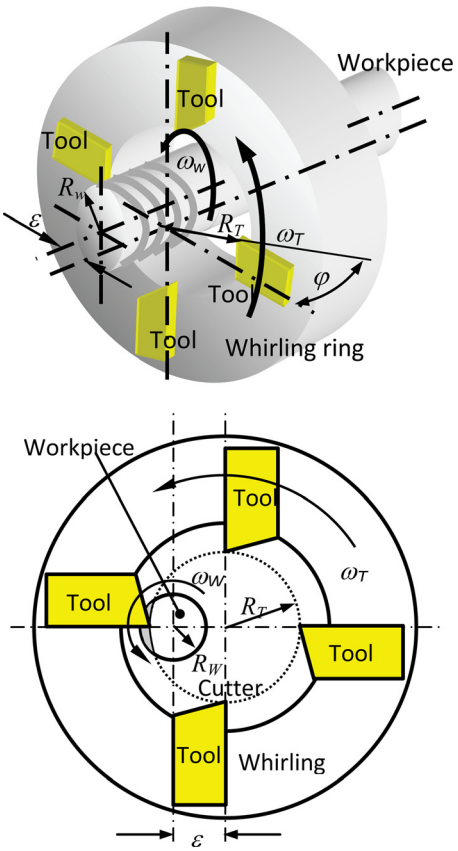

Fig. 1 Thread whirling

[1]Corresponding author.

Contributed by the Manufacturing Engineering Division of ASME for publication in the JOURNAL OF MICRO- AND NANO-MANUFACTURING. Manuscript received September 1, 2014; final manuscript received May 26, 2015; published online August 13, 2015. Assoc. Editor: Martin Jun.

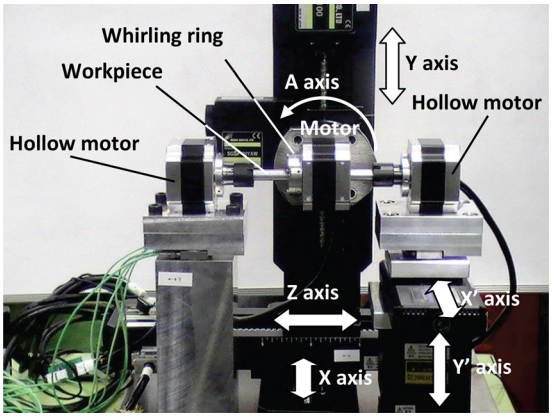

Fig. 2 Microwhirling machine tool

the uncut chip thickness in terms of the cutting parameters. The uncut chip thickness is discussed to validate its effect in the thread whirling of thin wires.

Whirling

Whirling is applied to machine screws by a combination of tool and workpiece rotations, as shown in Fig. 1. The cutting tools are clamped on the whirling ring at the radius R_T; and the ring rotates at the angular velocity ω_T. The workpiece with the radius R_W rotates at the angular velocity ω_W in the whirling ring with the eccentricity ε, which controls the depth of cut. In whirling, the workpiece rotating at a low revolution rate is cut by the cutting edges rotating at a high revolution rate. The lead of the screw is controlled by the inclination and the feed rate of the whirling ring with respect to the workpiece axis.

In turning a small diameter workpiece, the cutting speed is constrained to be low by the maximum limit of spindle speed and, as a consequence, the surface finish deteriorates. In whirling, the cutting speed is controlled by the rotation radius R_T and revolution rate ω_T of the cutting tools on the whirling ring. Therefore, a fine surface can be finished on a thin wire at a high cutting speed even though the maximum spindle speed is limited.

Because the tool and the workpiece rotate with eccentric centers, cutting and noncutting regimes alternate in whirling. Therefore, due to cooling during noncutting, the temperature rise of the tool edge is not so high. The material removal volume is also controlled to be small, as described later by the uncut chip thickness calculation model. The cutting force, thus, becomes small in interrupted cutting. Because the tool wear depends on the stress and the temperature [9], the tool wear is suppressed. Therefore, difficult-to-cut materials are machined with long tool lives in whirling.

Because interrupted cutting is performed in whirling, the chip formation is intermittent and the formed chips are short. Therefore, a fine surface is finished without scratching of the chips on the workpiece.

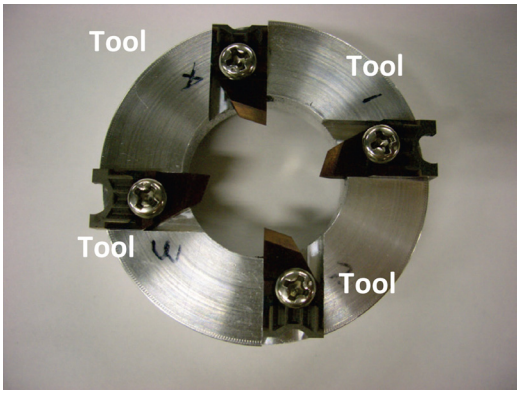

Fig. 3 Tool mounted on whirling ring

Micro whirling Machine Tool

Machine Tool Structure. Figure 2 shows the microwhirling machine developed for threading on thin wires with diameters of less than 1 mm. A workpiece is clamped by collets in two hollow motors. One of the motors is mounted on two linear stages (X'- and Y'-axis) for straightness adjustment of the workpiece clamping with respect to the feed of the whirling ring. A motor rotates the tools on the whirling ring. A rotation motor (A-axis) controls the inclination of the whirling ring; and three linear stages (X-, Y-, and Z-axis) control the cutting position and the feed of the whirling ring. The rotations of the whirling ring and the workpiece are controlled simultaneously, with the maximum spindle speed of the motors 4000 rpm.

The cutting tools are clamped on the whirling ring, as shown in Fig. 3. Because the tool edge alignment has an influence on the machining accuracy, the overhangs of the tools are adjusted with a device shown in Fig. 4. The workpiece is clamped in the opposed collets, as shown in Fig. 5(*a*). Workpiece vibration occurs because the stiffness of the thin wire is low and cutting is interrupted in the whirling process. In order to support the workpiece, two closely fitting polyurethane tubes are slid over it, one to each side of the cutting area. These are then clamped in a groove on a supporting metal bar that protrudes through the whirling ring, as shown in Fig. 5(*b*). This provides both high stiffness and damping for the workpiece.

Dynamic Response of Clamped Workpiece. Dynamic response tests were conducted to verify the effectiveness of the support system, as shown in Fig. 6. The displacement of the thin wire could not be measured because the measuring area was small and with rounded shape. Therefore, the amplitudes and the frequencies of vibrations of the collet clamping forces were compared for three different clamping conditions when an impulse force was generated at the center of the wire. A 0.49 N dead weight was hung from the wire by a thread. The impulse was generated by cutting the thread by a burner flame. The resulting vibrations in clamping force were measured with a piezoelectric dynamometer.

Figure 7 compares Y (axial) and Z (vertical) components of the clamping force vibration, as designated in Fig. 6. Figure 7(*a*)

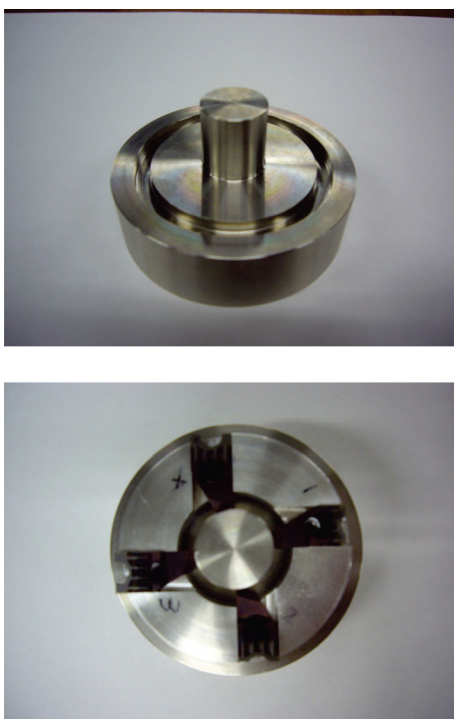

Fig. 4 Adjustment of edge alignment

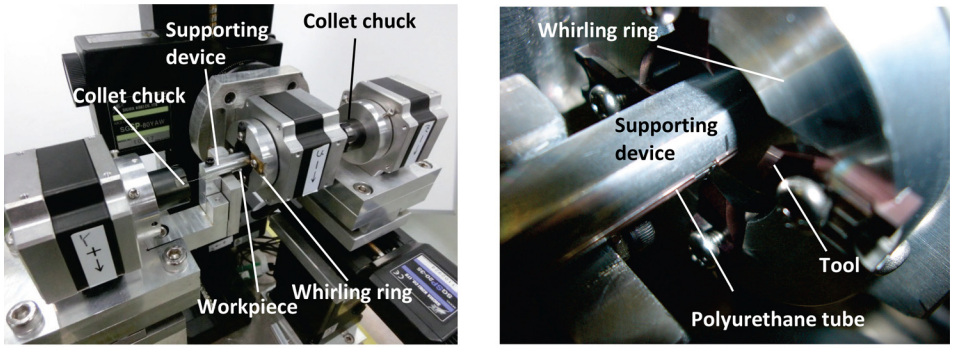

Fig. 5 Workpiece clamping system: (*a*) work area and (*b*) workpiece supporting device

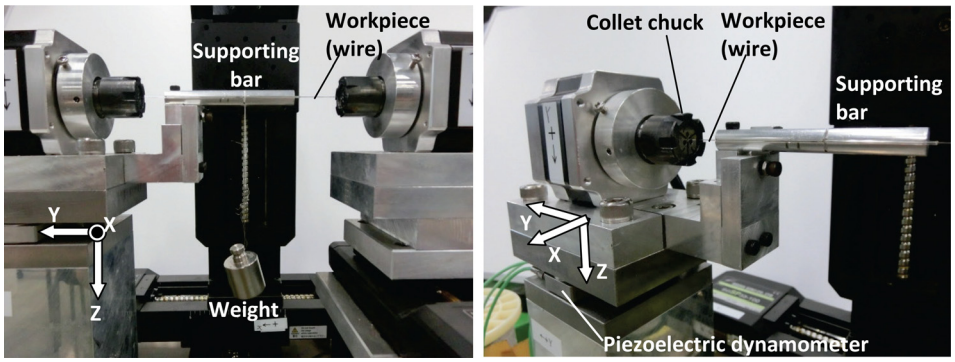

Fig. 6 Impulse response test

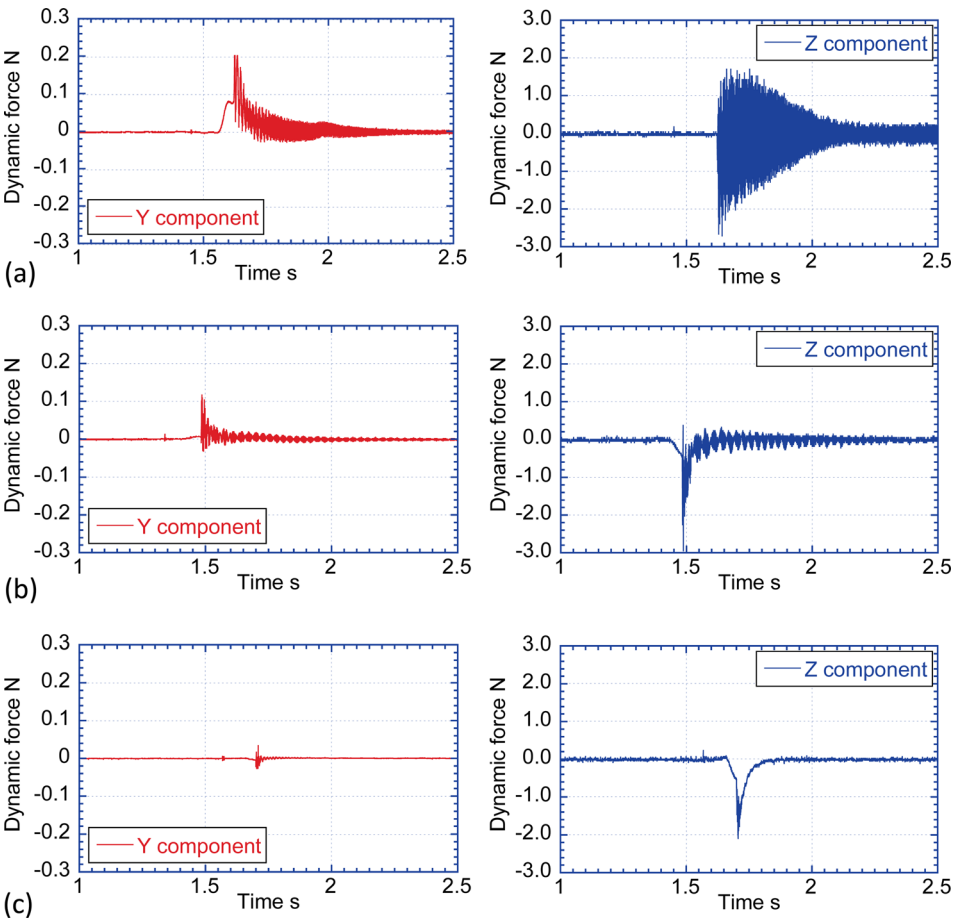

Fig. 7 Vibration in clamping force: (*a*) wire without supporting device, (*b*) wire clamped on supporting device, and (*c*) wire clamped on supporting device with polyurethane tubes

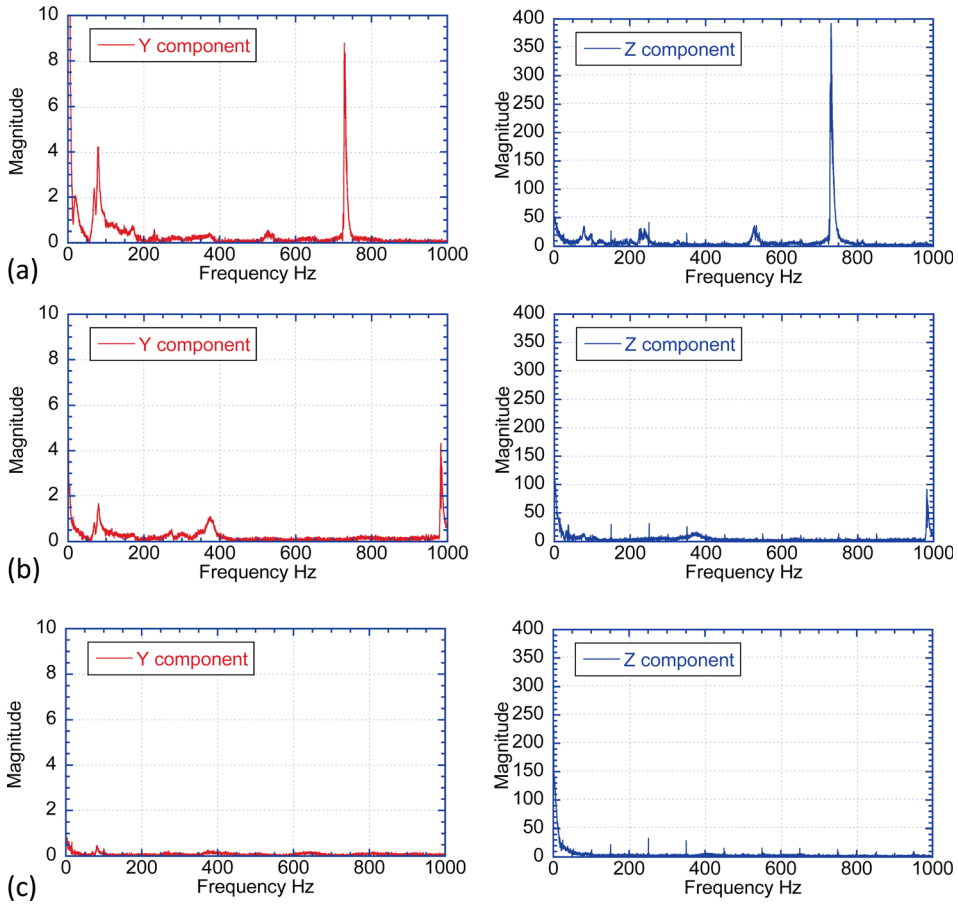

Fig. 8 Frequency analysis: (*a*) wire without supporting device, (*b*) wire clamped on supporting device, and (*c*) wire clamped on supporting device with polyurethane tubes

shows a natural vibration without the support device. Large amplitudes in *Y* and *Z* components are measured and the vibrations continue for a long time. Figure 7(*b*) shows the vibrations when the supporting metal bar without polyurethane tubes restricts the workpiece. The amplitude is restricted by contact with the groove on the supporting bar. The vibrations last for around 1 s. As may be seen in Fig. 7(*c*), support with the polyurethane tubes is effective in controlling the vibration of the thin wire. A small amplitude of the vibration and a high damping are measured. Figure 8 compares the frequency components of the vibrations. A large component at 730 Hz appears in the natural vibration of the thin wire, as shown in Fig. 8(*a*). The supporting bar reduces this and shifts it to the higher frequency of 982 Hz, as shown in Fig. 8(*b*). Figure 8(*c*) shows that supporting with the polyurethane tubes mounted on the supporting bar eliminates any prominent components. According to the model tests, the developed support system works well.

Uncut Chip Thickness Analysis

In order to support the choice of the cutting parameters in the cutting tests, the uncut chip thickness in the whirling process is considered here. Song and Zuo presented a model to obtain the uncut chip thickness in the general whirling process [6]. In line with the cutting demonstrated later in this study, a model is described for whirling without the inclination angle of the whirling ring here. In the model, only the locus of the cutting point at the center of the cutting edge is discussed. Tool geometry is ignored.

Tool Edge Motion. The workpiece rotates at the angular velocity ω_W in the actual cutting, as shown in Fig. 9(*a*). In the model,

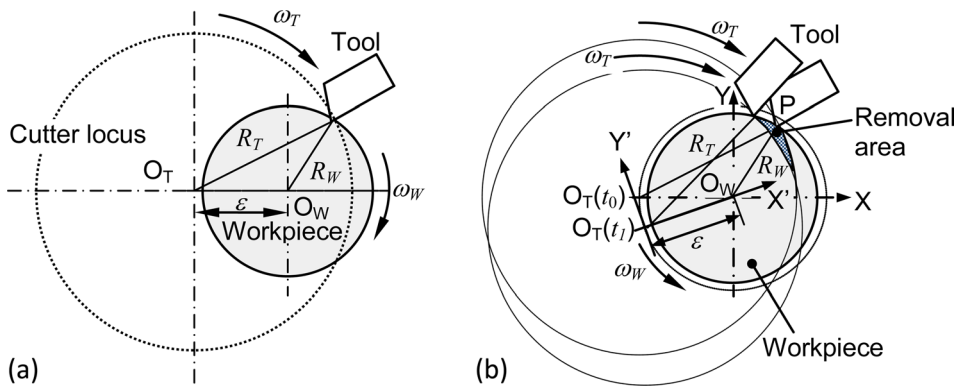

Fig. 9 Whirling process: (*a*) actual cutting in whirling and (*b*) analytical model of whirling

meanwhile, the workpiece does not rotate. Instead, the center of tool rotation O_T rotates around the workpiece at the radius ε at the angular velocity ω_W in the opposite direction to the tool rotating direction, as shown in Fig. 9(*b*). *X*–*Y*–*Z* is the reference coordinate system of the workpiece, where the origin O_W of *X*–*Y*–*Z* is the center of workpiece. *X*′–*Y*′–*Z*′ is the coordinate system of the tool rotating around O_W and moving along the workpiece axis, *Z*. Then, the tool rotates at the angular velocity ω_T in the coordinate system *X*′–*Y*′–*Z*′.

The coordinates (x', y', and z') of a point *P* on an edge change with the cutting time *t*

$$\begin{bmatrix} x' \\ y' \\ z' \end{bmatrix} = \begin{bmatrix} R_T \cos \omega_T t + \varphi \\ R_T \sin \omega_T t + \varphi \\ 0 \end{bmatrix} \tag{1}$$

where φ is the angular position of the cutting edge. For example, when four edges are mounted on the whirling ring, the angles are 0, $\pi/2$, π, and $3\pi/2$, respectively. ω_T is negative because the rotating direction is clockwise in Fig. 9. Because the origin O_T of *X*′–*Y*′–*Z*′ rotates around the center of the workpiece O_W at the radius ε at the counterclockwise angular velocity ω_W and moves along the *Z*-axis at the feed rate *f*, the point *P* on the edge in *X*–*Y*–*Z* is transformed as

$$\begin{bmatrix} x \\ y \\ z \end{bmatrix} = \begin{bmatrix} \cos \omega_W t & -\sin \omega_W t & 0 \\ \sin \omega_W t & \cos \omega_W t & 0 \\ 0 & 0 & 1 \end{bmatrix} \begin{bmatrix} x' \\ y' \\ z' \end{bmatrix} + \begin{bmatrix} -\varepsilon \cos \omega_W t \\ -\varepsilon \sin \omega_W t \\ ft \end{bmatrix} \tag{2}$$

The material is removed when the rotation radius of *P* in *X*–*Y*–*Z* is less than the workpiece radius R_W

$$\sqrt{x^2 + y^2} \le R \tag{3}$$

Therefore, the cutting area is determined by Eqs. (2) and (3).

Uncut Chip Thickness

Figure 10 shows the cutting area divided into regions *A*–*B* and *B*–*C*. In region *A*–*B*, the uncut chip thickness is given by the cutting position *P* and a point Q_1 on the workpiece surface. In region *B*–*C*, the uncut chip thickness is given by *P* and a point Q_2 on the locus of the previous edge at the prior angle γ. γ is the difference between the angular positions φ. For example, when four edges are mounted on the whirling ring, the angle γ is $\pi/2$. Because Q_1 or Q_2 is located on the extension line of O_TP, the cutting thickness is given by PQ_1 or PQ_2. Q_1 or Q_2 is given by

$$\begin{bmatrix} x \\ y \\ z \end{bmatrix} = \begin{bmatrix} \cos \omega_W t & -\sin \omega_W t & 0 \\ \sin \omega_W t & \cos \omega_W t & 0 \\ 0 & 0 & 1 \end{bmatrix} \begin{bmatrix} \xi \cos \omega_T t + \varphi \\ \xi \sin \omega_T t + \varphi \\ 0 \end{bmatrix} + \begin{bmatrix} -\varepsilon \cos \omega_W t \\ -\varepsilon \sin \omega_W t \\ ft \end{bmatrix} \tag{4}$$

where ξ is the parameter that determines Q_1 or Q_2. When material is removed, ξ is larger than R_T. In region *A*–*B*, ξ at Q_1 is determined by the following equation of the workpiece surface and Eq. (4):

$$\begin{bmatrix} x \\ y \\ z \end{bmatrix} = \begin{bmatrix} R_W \cos \theta \\ R_W \sin \theta \\ ft \end{bmatrix} \tag{5}$$

where θ is the angle of Q_1 in the workpiece coordinate system *X*–*Y*–*Z*.

In region *B*–*C*, the previous edge at the prior angle γ is given at a time of $t - \gamma/\omega_T + \Delta t$

$$\begin{bmatrix} x \\ y \\ z \end{bmatrix} = \begin{bmatrix} \cos\omega_W(t-\gamma/\omega_T+\Delta t) & -\sin\omega_W(t-\gamma/\omega_T+\Delta t) & 0 \\ \sin\omega_W(t-\gamma/\omega_T+\Delta t) & \cos\omega_W(t-\gamma/\omega_T+\Delta t) & 0 \\ 0 & 0 & 1 \end{bmatrix} \times \begin{bmatrix} R_T\cos\omega_T(t-\gamma/\omega_T+\Delta t)+\varphi \\ R_T\sin\omega_T(t-\gamma/\omega_T+\Delta t)+\varphi \\ 0 \end{bmatrix} + \begin{bmatrix} -\varepsilon\cos\omega_W(t-\gamma/\omega_T+\Delta t) \\ -\varepsilon\sin\omega_W(t-\gamma/\omega_T+\Delta t) \\ f(t-\gamma/\omega_T+\Delta t) \end{bmatrix} \tag{6}$$

where Δt is determined so that Q_2 is on the extension of line O_TP. ξ at Q_2 is determined to satisfy Eqs. (4) and (6). Because the feed along *Z*-axis is very small in one revolution, it is ignored and ξ is determined in *X*–*Y* plane. The uncut chip thickness is given by the following equation with the determined ξ:

$$t_1 = \xi - R_T \tag{7}$$

Figure 11 shows the change in the uncut chip thickness in *X*–*Y* plane when a screw is machined on a 0.3 mm diameter wire.

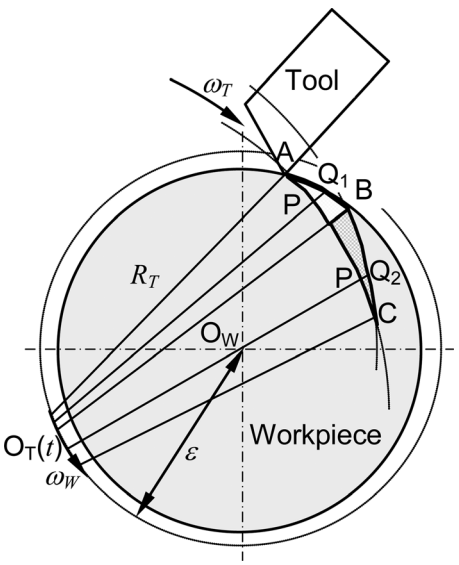

Fig. 10 Cutting area in whirling

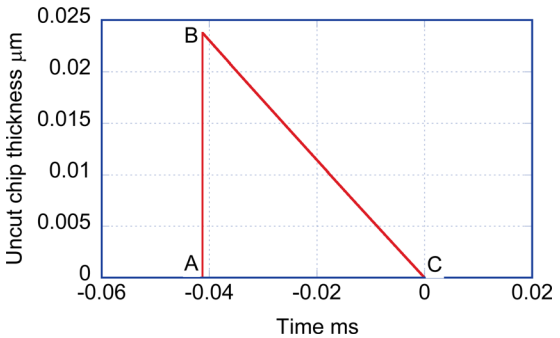

Fig. 11 Uncut chip thickness

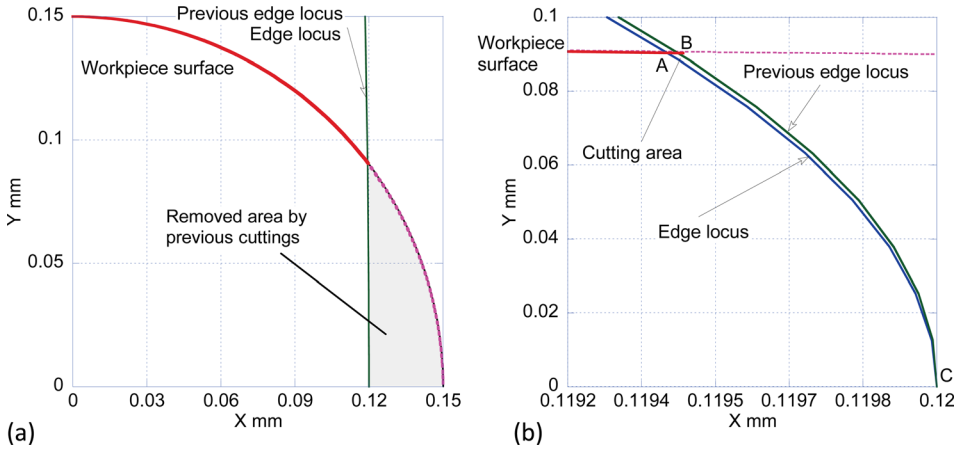

Fig. 12 Locus of tool motion with workpiece surface: (*a*) in a quarter of workpiece and (*b*) magnified

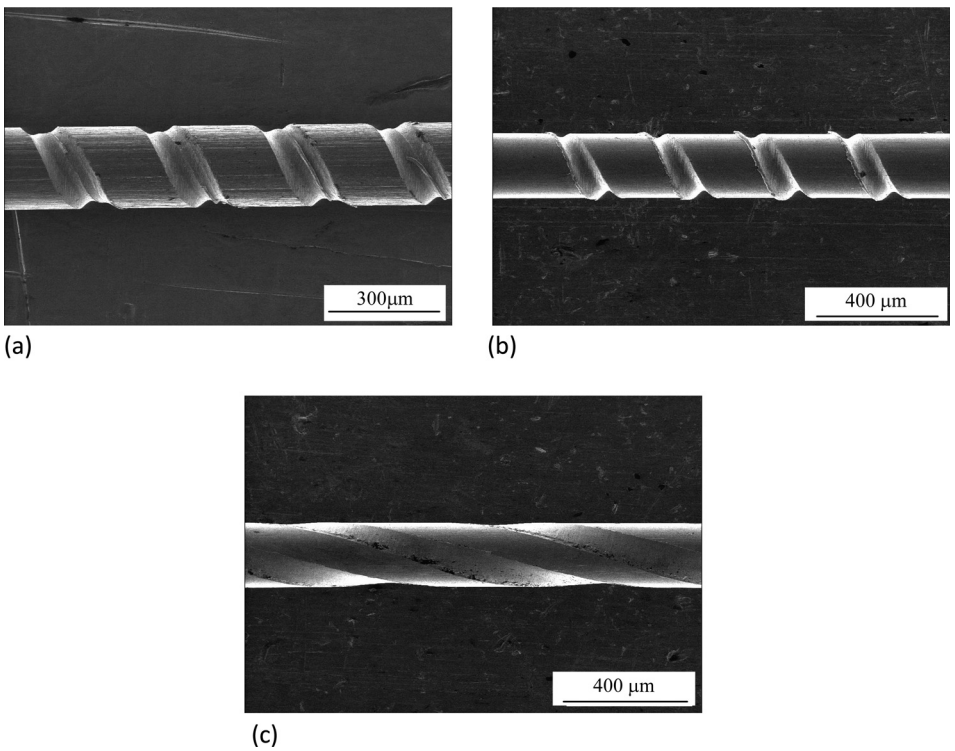

Fig. 13 Machining examples: (*a*) example 1, (*b*) example 2, and (*c*) example 3

Workpiece revolution speed is 0.5 rpm and four cutting tools, mounted on a whirling ring, rotate at 3000 rpm at a rotation radius of 14 mm. The feed rate is 0.2 mm/min. The depth of cut is 30 μm with an eccentricity of 6.88 mm. Figure 12(*a*) shows a quarter of the workpiece. At this scale, the cutting area is small. Figure 12(*b*) shows the magnified figure. The cutting edge penetrates into the workpiece at *A*; passes *B* at the maximum uncut chip thickness; and exits from the workpiece at *C*. From *A* to *B*, the removed area is between the workpiece surface and the locus of the tool. The uncut chip thickness increases at a high rate of change over the time (Fig. 11) from −0.04128 ms to −0.04125 ms. Then, from *B* to *C*, the removed area is between the loci of the tool and the previous tool. The uncut chip thickness gradually decreases after −0.04125 ms, as shown in Fig. 11. The analysis here is for cuts other than the first cut. The uncut chip thickness is actually 30 μm at the first engagement of an edge into the workpiece because the uncut chip thickness is determined only by the area between

Table 1 Cutting parameters

	Example 1	Example 2	Example 3
Workpiece	Ti-6Al-4 V	Stainless steel	Stainless steel
Workpiece diameter		0.3 mm	
Workpiece revolution		0.5 rpm	
Tool		TiAlN coated carbide tool	
Tool wedge angle		60 deg	
Tool rake angle		0 deg	
Number of tools	4	1	1
Tool rotation diameter		14 mm	
Tool spindle speed		3000 rpm	
Feed rate		0.2 mm/min	1.0 mm/min
Depth of cut		30 μm	40 μm
Lubrication		Dry	

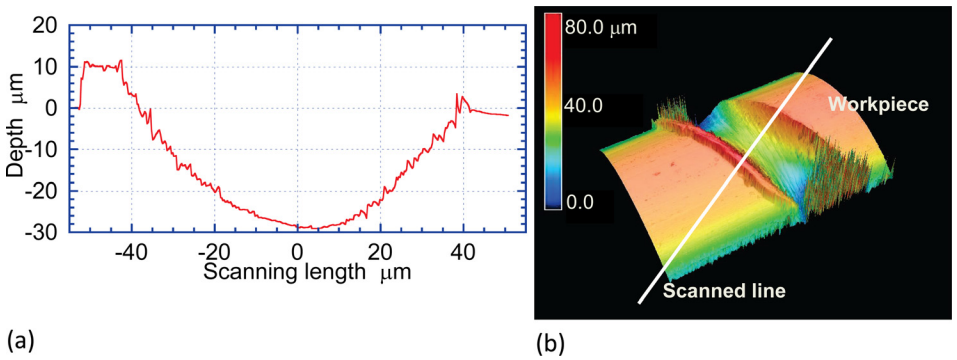

Fig. 14 Surface profile: (*a*) profile and (*b*) three-dimensional image

the workpiece surface and the locus of the tool. After the second engagement of the edge, the maximum uncut chip thickness is no more than 0.02376 μm. This is much smaller than the depth of screw of 30 μm. According to the research in microcutting [10], chips form when the uncut chip thickness is more than "minimum chip thickness." Because the analyzed cutting thickness, 0.02376 μm, is much smaller than the minimum chip thickness, material removal is expected to occur for only some cuts of the edges. The analysis supports the choice of cutting parameters for small cutting forces associated with the cutting thicknesses.

Cutting Tests

Figure 13 shows examples of microthread whirling on titanium alloy (Ti-6Al-4 V) and stainless steel wires, where the diameters are 0.3 mm. The threads were machined with single point tools with a wedge angle of 60 deg. The tool material was TiAlN coated carbide. Table 1 shows the cutting parameters that were used. Figure 13(*a*), example 1 shows serration on the surface finish within a screw cut by four edges. Although the alignment of the four edges is controlled in the radial direction, as shown in Fig. 4, there is alignment error in the axial direction. This induces the serration. Figure 13(*b*), example 2 shows a screw cut on stainless steel wire by one edge. Figure 14(*a*) shows the surface profile along the line designated in Fig. 14(*b*). The surface profile is measured with a laser confocal microscope. Although burr formation at a height of 10 μm is observed at the left side of the groove, the depth of groove is as specified. It demonstrates the effectiveness of the high stiffness of the workpiece support system. The presented whirling also enables a high lead screw to be machined at a feed rate of 2.0 mm/rev (1.0 mm/min), as shown in example 3 of Fig. 13(*c*).

Because the cutting speeds depend on the rotation diameters of the tools on the whirling ring, surfaces are finished at high cutting speeds. The cutting speeds of these examples are 132 m/min at a tool rotation diameter of 14 mm and a spindle speed of 3000 rpm. In turning, a spindle speed of 140,056 rpm would be required to give same cutting speed for the 0.3 mm diameter workpiece. The groove shapes in whirling are uniform without adhesion of the chips. These examples prove that whirling is effective in microthreading with the presented supporting device of the workpiece.

Conclusions

Whirling has been applied to machining of microscrews on thin wires. In the whirling cut, the workpiece and the tool rotate with an eccentricity of their centers. Because the material is removed in a small volume at a high cutting speed, the whirling has advantages in surface finish, tool wear, and chip control compared to turning.

A microwhirling machine tool has been developed for machining of the microgrooves on the thin wires with diameters of less than 1 mm. In order to improve the stiffness and the damping of the workpiece, the wire, which is clamped between collets, is also supported on a metal bar by inserting it into a closely fitting polyurethane tube. Dynamic response tests have been conducted to verify the effect of the supporting system. The amplitudes and the frequencies of the vibrations of the collet clamping forces were measured when impulse forces were loaded at the center of the wire. They show the effectiveness of the supporting system in suppressing the vibration.

A mechanistic model is applied to consider the small uncut chip thickness. Microgrooves have been machined on 0.3 mm diameter titanium alloy and stainless steel wires. Because a high cutting speed can be maintained by the rotation radius of the tool, the surface finish is improved without adhesion of the chips. In the presented machining example, the uncut chip thickness is much smaller than the depth of the groove. Because the uncut chip thickness is associated with the cutting force, the specified depth of groove is generated with a small cutting force, with a high stiffness of workpiece holding system.

References

[1] Cheng, K., and Huo, D., 2013, *Micro-Cutting: Fundamentals and Applications*, Wiley, Hoboken, NJ.

[2] Vollertsen, F., Hu, Z., Niehoff, H. S., and Theiler, C., 2004, "State of the Art in Micro Forming and Investigations Into Micro Deep Drawing," J. Mater. Process. Technol., **151**(1–3), pp. 70–79.

[3] Yokoyama, K., Ichikawa, T., Murakami, H., Miyamoto, Y., and Asaoka, K., 2002, "Fracture Mechanisms of Retrieved Titanium Screw Thread in Dental Implant," Biomaterials, **23**(12), pp. 2459–2465.

[4] Mohan, L. V., and Shunmugam, M. S., 2007, "Simulation of Whirling Process and Tool Profiling for Machining of Worms," J. Mater. Process. Technol., **185**(1–3), pp. 191–197.

[5] Lee, Y. M., Choi, W. S., Son, J. H., Oh, K. J., Kim, S. I., Park, G. W., and Jung, H. C., 2008, "Analysis of Worm Cutting Characteristics in Whirling Process," Mater. Sci. Forum, **575–578**, pp. 1402–1406.

[6] Song, S. Q., and Zuo, D. W., 2014, "Modeling and Simulation of Whirling Process Based on Equivalent Cutting Volume," Simul. Modell. Pract. Theory, **42**, pp. 98–106.

[7] Son, J. H., Han, C. W., Kim, S. I., Jung, H. C., and Lee, Y. M., 2010, "Cutting Force Analysis in Whirling Process," Int. J. Mod. Phys. B, **24**(15–16), pp. 2786–2791.

[8] Guo, Q., Wang, Y. L., Feng, H. T., and Li, Y., 2012, "Establishment of Cutting Tools' Processing Angle Model in Whirling Milling," Adv. Mater. Res., **433–440**, pp. 635–641.

[9] Usui, E., Shirakashi, T., and Kitagawa, T., 1984, "Analytical Prediction of Tool Wear," Wear, **100**(1–3), pp. 129–151.

[10] Chae, J., Park, S. S., and Freiheit, T., 2006, "Investigation of Micro-Cutting Operations," Int. J. Mach. Tools Manuf., **46**(3–4), pp. 313–332.